Radiation Physics and Chemistry 203 (2023) 110595

Contents lists available at ScienceDirect

Radiation Physics and Chemistry

journal homepage: www.elsevier.com/locate/radphyschem

Angular distribution of characteristic X-rays following electron impact ionization

Daniel Pinheiro *, Pedro Amaro *, Jorge Machado, Mauro Guerra, José Paulo Santos

Laboratory of Instrumentation, Biomedical Engineering and Radiation Physics (LIBPhys-UNL), Department of Physics, NOVA School of Science and Technology, NOVA University Lisbon, 2829-516 Caparica, Portugal

ARTICLE INFO

Keywords:
Angular distribution
Atomic processes
Fundamental parameters
Atomic data
Synthetic spectra
Electron impact ionization

ABSTRACT

In this paper, we present a theoretical study of the X-ray fluorescence emission after vacancy of K-shell due to electron impact ionization. In particular, we focus on the angular distributions of the characteristic Kα emission lines following this process. Rh was chosen for the analysis since it is a common element in X-ray tube anodes. In this analysis we also considered some elements along the period-4, i.e., Ni, Cu and Co as case-studies. In doing so, we studied the magnetic sub-level population of the ionized states, which is directly related to the angular distribution of the emission. A relative low angular distribution for the Kα emission of Rh of 0.5% was observed, which makes the assumption of isotropic emission correct for most studies. Moreover, a comparison with the respective angular emission for adjacent elements in the fourth period of the periodic table shows that this isotropy is attributed to a small total angular momentum of the resulting configurations after ionization, as well as to opposite angular distributions of the various transitions, which average to a maximum of 0.7% angular asymmetry in Ni.

1. Introduction

The ionization of a K-shell electron in light to medium weight atoms by incident electrons and subsequent X-ray emission are the fundamental atomic processes taking place at X-ray tube anodes. Since most X-ray spectroscopy based techniques have X-ray tubes as a primary X-ray source, accurate analysis of these processes are warranted not only to calibrate instruments, but also to improve the technique's reliability. This need of improvement is even more pertinent for semiconductor fabrication and characterization, since uncertainties in the atomic fundamental parameters prevent further advances in structural analysis of materials based on X-ray techniques (Rousseau, 2001; Guerra et al., 2015b). Accurate values of fundamental parameters enable a precise detachment of condensed matter and chemical subtle effects from the dominant atomic processes in X-ray emission, which overall benefits all material characterization based on X-ray spectroscopy. Therefore, atomic fundamental parameters must be benchmarked with up-to-date uncertainties in order to further improve any spectroscopy analysis (Ménesguen et al., 2018).

Due to this motivation, fundamental parameters such as fluorescence yields, line energies, widths and ratios have been remeasured and recalculated over the last decade, overcoming the large uncertainties and discrepancies previously observed in the literature (Sampaio et al., 2014; Guerra et al., 2015b; Martins et al., 2020a,b; Guerra et al., 2021).

While most of this research was focused on the total X-ray emission obtained from these fundamental parameters, no attention was given to the respective angular distribution of the emission, i.e., it is assumed to be isotropic. This may be relevant since most spectroscopy observations have a defined geometry for the incident particles and X-ray detection. To fulfil this lack, we evaluate the angular distribution of the X-ray emission after relevant atomic processes. Note that in experimental measurements there is always an angular distribution due to angular-dependent absorption effects for both the incident electrons and emitted X-rays (e.g. Singh et al. (2017)). However, the focus of this work is on the *ab initio* angular emission of the atomic process and not on the geometrical absorption effects. As we shall see, assuming isotropy is a good approximation for most cases, however further improvement of X-ray metrology will need this effect to be considered eventually.

Since the last decades, there has been extensive experimental and theoretical research in these angular correlation phenomena on X-ray emission. While almost all works focused on photoionization from synchrotron radiation (Schmidt, 1992; Yamaoka et al., 2002; Tartari et al., 2003; Kust et al., 2003; Barrea et al., 2005; Santra et al., 2007; Namito et al., 2008; Gonzales et al., 2011; Kumar et al., 2008; Karanfil and Barrea, 2011; Zhang et al., 2020), few other atomic processes were also considered, namely nuclear electron capture (Han and Demir,

* Corresponding authors.
E-mail addresses: ds.pinheiro@campus.fct.unl.pt (D. Pinheiro), pdamaro@fct.unl.pt (P. Amaro).

https://doi.org/10.1016/j.radphyschem.2022.110595
Received 16 September 2021; Accepted 9 October 2022
Available online 14 October 2022

2011) and electron impact ionization (Sestric et al., 2014). All this research covers both electron–photon and photon–photon angular correlation for radiative emission. Additionally, research on the angular distribution and spin polarization of Auger electron emission is also present (Nishimura et al., 1986; Blum and Kleinpoppen, 1979; Scofield, 1976; Yamaoka et al., 2002; Barrea et al., 2005; Chen and Reed, 1994; Kabachnik and Sazhina, 1984; Tulkki et al., 1993). This research encompasses low atomic numbers such as He, Li, Na, Mg (Blum and Kleinpoppen, 1979), metals such as Fe, Zn and Mo (Scofield, 1976), noble gases such as Ar, Xe, Kr (Tulkki et al., 1993; Nishimura et al., 1986), as well as high atomic numbers such as W, Er, Au, Pb and U (Scofield, 1976; Barrea et al., 2005; Yamaoka et al., 2002; Zhang et al., 2020). The specimens studied also range from neutral systems to highly charged ions (Chen and Reed, 1994; Sharma et al., 2010; Wu et al., 2014; Shah et al., 2018; Amaro et al., 2017). While these works show a variety of atomic systems and processes, the general theoretical formalism of polarization and angular distributions are well described by density-matrix theory (Balashov et al., 2000).

Besides neutral atoms, further research has been done on angular correlations on atomic processes that only occur on highly charged ions, such as hyperfine-induced transitions (Chen and Dong, 2018; Wu et al., 2020), radiative electron capture (Tashenov et al., 2006; Wu et al., 2014), electron impact excitation (Wu et al., 2020, 2021) and dielectronic recombination (Nakamura et al., 2011; Amaro et al., 2017; Shah et al., 2018; Iorga and Stancalie, 2019).

To the best of our knowledge, few works calculated the angular distribution of X-rays after electron impact ionization. In case of Au, Sestric et al. (2014) found that Lα and Lβ emission is isotropic while Lγ X-rays exhibits weak anisotropy. This was further confirmed by Barros et al. (2019) with a comprehensive theoretical and experimental work, also for Ta and W. The angular distribution of L X-rays was also explored for the case of Ag by Wang et al. (2016) and Liu et al. (2019) for different incident electron energies, showing that Lβ1, and Lγ1 X-rays are isotropic, while the Lα X-rays exhibit anisotropic emission, as well as Lβ2 having some energy-dependent anisotropy.

In this work, we investigate the angular distribution of Kα emission, following electron impact ionization at an incident energy of 40 keV for several elements as case studies. We consider Rh and near elements in the periodic table, namely Co, Ni and Cu. Both the synthetic spectra and angular distributions were theoretically calculated, and a full comparison between isotropic and anisotropic emission is presented.

2. Theory

2.1. Synthetic spectra

We construct a synthetic spectra by evaluating the line intensity of all the radiative transitions from the initial ionized level i towards a final level f with Kα transition, which is given by

$$I_{if} = \sigma_i \omega_i = \sigma_i \frac{W_{if}^R}{W_i^R + W_i^{NR}} \Omega_{if}(\vartheta). \quad (1)$$

This line intensity is the electron impact cross-section σ_i to form the ionized level i, weighted by the transition fluorescence yield ω_i, which is the probability that the K-shell hole in level i is filled through Kα emission, and corrected by the angular distribution $\Omega_{i,f}(\vartheta)$ (further details in Section 2.4). The term W_{if}^R stands for the radiative transition rate of the initial i to the final f states, while W_i^R and W_i^{NR} stand for the total radiative $W_i^R = \sum_j W_{ij}^R$ and radiationless $W_i^{NR} = \sum_{j'} W_{ij'}^{NR}$ transition rates. Here, the summation over j for the total radiative rate addresses all final levels with a vacancy above the K-shell, while for the radiationless case, the index j' corresponds to all energy-allowed Auger paths. We also attribute a Lorentzian to each line intensity, being centred at the transition energy and having a width given by

$$\Gamma_{if} = \Gamma_i + \Gamma_f, \quad (2)$$

where $\Gamma_i = \hbar\left(W_i^R + W_i^{NR}\right)$ and $\Gamma_f = \hbar\left(W_f^R + W_f^{NR}\right)$.

2.2. MCDF

Following previous works (e.g. Guerra et al. (2021)) all the transition energies, radiative and Auger rates necessary to evaluate the line intensities and respective positions, were evaluated from calculations, employing the state-of-the-art multiconfiguration Dirac–Fock (MCDF) method. In this method, the electronic correlation is included by writing the atomic antisymmetric wave function ψ as a linear combination of the φ configuration state functions: $\psi(1, 2, \ldots, N) = \sum_i a_i \varphi_i$, where a_i are mixing coefficients.

The relativistic general purpose multiconfiguration Dirac–Fock code (MCDFGME) developed by J. P. Desclaux, P. Indelicato and co-authors (Desclaux, 1975; Indelicato and Desclaux, 1990; Indelicato et al., 2007; Santos et al., 2005) implements the MCDF method, using a self-consistent field approach. Various contributions are included in the self-consistent calculation, such as Coulomb and Breit (magnetic and retardation parts), both containing direct and exchange components, as well as quantum electrodynamics (QED) local potentials, such as vacuum polarization. Other QED contributions, such as self-energy, are also included as perturbations.

For the calculation of radiative rates, the optimized-level method was used to calculate the wave functions and energies of both the initial and final states considering full relaxation. As each state was optimized separately, they are non-orthogonal and to calculate radiative rates, the formalism described by Löwdin (1955) was used in the MCDFGME code. Moreover, the length gauge was considered for all radiative transition rates. In case the of radiationless rates, the continuum-electron wavefunctions are obtained by solving the Dirac–Fock equations with the same atomic potential of the initial state. Here, no relaxation was allowed in both initial and final states of the Auger process.

Due to the amount of energy levels, the calculation was used in the single-configuration approach.

2.3. Electron impact ionization

The necessary electron impact ionization cross sections were calculated using the Flexible Atomic Code (FAC) developed by Gu (2008). This code uses the relativistic configuration-interaction approach in an optimized local potential of all electrons. For continuum processes, such as the electron impact ionization required in this work, FAC uses the distorted wave (DW) approximation. A few cases were verified with the effective formula from the Modified Relativistic Binary Encounter Bethe model (Guerra et al., 2012, 2015a), giving agreement in the quoted precision for all results listed in this work. Additionally, FAC provides electron impact ionization cross sections for each magnetic sublevel, which are needed to calculate the angular distributions presented in this work. Version 1.1.5 of FAC was used in the calculations.

2.4. Angular distribution

We follow the theory described in Balashov et al. (2000) for the angular distribution of photons emitted from an excited or ionized state resulting from a collision, such as,

$$A'(\alpha' J') + e^- \longrightarrow A^*(\alpha_i J_i) \longrightarrow A(\alpha_f J_f) + \gamma. \quad (3)$$

The atomic levels before and after the collision, as well as after decay are represented by A', A^* and A respectively. The necessary set of quantum numbers to uniquely identify each quantum level, apart from the total angular momentum J, are denoted by α.

Incident electrons with a defined direction often lead to excited (or ionized) states that are aligned along this direction, i.e., contains an unbalanced population of magnetic sublevels not statistically distributed.

Table 1
Ground levels and ionized levels in jj-coupled notation considered in the calculation and the respective alignment parameter $\mathcal{A}_2(\alpha_i J_i)$.

Atom	Ground level	J'	Ionized level	J_i	α_i	$\mathcal{A}_2(\alpha_i J_i)$
Cu	$[3d^{10}\ 4s]_{1/2}$	1/2	$[1s\ 4s]_1$	1	0	0[a]
			$[1s\ 4s]_0$	0	0	0
Co	$[(3d^3_{3/2})_{3/2}(3d^4_{5/2})_4\ 4s^2]_{9/2}$	9/2	$[(1s(3d^3_{3/2})_{3/2})_2\ (3d^4_{5/2})_4]_4$	4	0	0.063308
			$[(1s(3d^3_{3/2})_{3/2})_1(3d^4_{5/2})_4]_4$	4	1	0.063311
			$[(1s(3d^3_{3/2})_{3/2})_2(3d^4_{5/2}]_2]_4$	4	2	0.063313
			$[(1s(3d^3_{3/2})_{3/2})_2(3d^4_{5/2})_4]_5$	5	0	0.051467
			$[(1s(3d^3_{3/2})_{3/2})_1(3d^4_{5/2})_4]_5$	5	1	0.051461
Rh	$[((4d^3_{3/2})_{3/2}\ (4d^5_{5/2})_{5/2})_4\ 5s]_{9/2}$	9/2	$[((1s(4d^3_{3/2})_{3/2})_2(4d^5_{5/2})_{5/2})_{7/2}5s]_4$	4	0	0.063311
			$[((1s(4d^3_{3/2})_{3/2})_1(4d^5_{5/2})_{5/2})_{7/2}5s]_4$	4	1	0.063310
			$[((1s(4d^3_{3/2})_{3/2})_2(4d^5_{5/2})_{5/2})_{9/2}5s]_4$	4	2	0.063311
			$[((1s(4d^3_{3/2})_{3/2})_2(4d^5_{5/2})_{5/2})_{9/2}5s]_5$	5	0	0.051465
Ni	$[(3d^3_{3/2})_{3/2}\ (3d^5_{5/2})_{5/2}\ 4s^2]_4$	4	$[(1s(3d^3_{3/2})_{3/2})_2(3d^5_{5/2})_{5/2}]_{7/2}$	7/2	0	−0.109104
			$[(1s(3d^3_{3/2})_{3/2})_1(3d^5_{5/2})_{5/2}]_{7/2}$	7/2	1	−0.109116
			$[(1s(3d^3_{3/2})_{3/2})_2(3d^5_{5/2})_{5/2}]_{9/2}$	9/2	0	−0.110093

[a]Within the table accuracy.

This unbalanced distribution is quantified by the alignment parameters defined given by

$$\mathcal{A}_k(\alpha_i J_i) = \frac{\sqrt{2J_i+1}}{\sigma(\alpha_i J_i)} \times \sum_{M_i=-J_i}^{M_i=J_i} (-1)^{J_i-M_i}\,\langle J_i M_i, J_i - M_i | k0\rangle\,\sigma(\alpha_i J_i M_i) \tag{4}$$

The $\sigma(\alpha_i J_i M_i)$ stands for the collision cross section for each $\alpha_i J_i$ level's magnetic sublevel. The total cross section for each $\alpha_i J_i$ level is given by $\sigma(\alpha_i J_i) = \sum_{M_i} \sigma(\alpha_i J_i M_i)$, which in the present case is the ionization cross-section $\sigma(\alpha_i J_i) \equiv \sigma_i$. Alignment parameter are often used to describe the angular distribution of photons of aligned states, which is given by

$$\Omega_{if}(\vartheta) = \frac{1}{4\pi}\left[1 + \sum_{k=2,4,\ldots} \alpha_k^{if}\,\mathcal{A}_k(\alpha_i J_i) P_k(\cos\vartheta)\right]. \tag{5}$$

Here, $P_k(\cos\vartheta)$ is a set Legendre polynomials, containing the dependency on the angle ϑ of observation with respect to the electron incident direction.

In this work, we consider only the dominant allowed (electric dipole) transitions, the incident electrons to be non-polarized, as well as a polarization insensitive detector, which is common setting in almost all X-ray experiments.

In this case only the alignment parameter $\mathcal{A}_k(\alpha_i J_i)$ with $k = 2$ given by

$$\mathcal{A}_2(\alpha_i J_i) = \left[\frac{5}{(2J_i+3)J_i(J_i+1)(2J_i-1)}\right]^{1/2} \times \frac{1}{\sigma(\alpha_i J_i)} \sum_{M_i} [3M_i^2 - J_i(J_i+1)]\sigma(\alpha_i J_i M_i). \tag{6}$$

can be non-zero. The intrinsic anisotropy parameter with $k = 2$ for photon emission in dipole approximation, α_2^{if}, is given by

$$\alpha_2^{if} = \sqrt{\frac{3}{2}}(2J_i+1)(-1)^{J_i+J_f+3}\begin{Bmatrix} J_i & J_i & 2 \\ 1 & 1 & J_f \end{Bmatrix}. \tag{7}$$

This coefficient only depends on the total angular momentum of the decay matrix elements in the dipole approximation.

3. Results and discussion

In this work, we considered four elements, namely Cu, Ni, Co and Rh, for the angular distribution of the Kα_1 and Kα_2 emission manifolds. For the cases of Ni, Co and Rh, the Kα_1 and Kα_2 lines manifolds comprise a large number of lines of approximately 10 000 for Ni, 72 000 for Co and 24 000 for Rh due to the open $3d$ and $4d$ shells, while in the case of Cu, the initial valence configuration is $4s$ and the Kα lines contain much fewer lines.

Table 2
Anisotropy parameters α_2^{if} for emitted dipole photons that were used in the calculation.

J_i	J_f	α_2^{if}	J_i	J_f	α_2^{if}
0	1	0	1	0	$1/\sqrt{2}$
1	1	$-1/2\sqrt{2}$	1	2	$1/10\sqrt{2}$
4	3	$\sqrt{11}/4\sqrt{7}$	5	4	$\sqrt{858}/30$
4	4	$-\sqrt{77}/20$	5	5	$-\sqrt{858}/20$
4	5	$\sqrt{7}/5\sqrt{11}$	5	6	$\sqrt{858}/52$
7/2	5/2	$\sqrt{3}/2\sqrt{7}$	9/2	7/2	$\sqrt{11}/2\sqrt{30}$
7/2	7/2	$-2/\sqrt{21}$	9/2	9/2	$-4\sqrt{2}/\sqrt{165}$
7/2	9/2	$\sqrt{7}/10\sqrt{3}$	9/2	11/2	$\sqrt{33}/11$

We calculated the Kα_1 and Kα_2 synthetic spectra for these four elements, using Eqs. (1) and (2) and transition energies from the MCDFGME code. Each line was represented by a Lorentzian distribution according to the calculated intensity, width and position. The final spectrum was constructed by summing all of these Lorentzian lines.

Afterwards, we calculated the angular distribution of the dipole radiation emitted from each of these transitions. These angular distributions were obtained for electron impact ionization of the K shell at 40 keV, in accordance to the excitation mechanism used in the synthetic spectra previously calculated. Additionally, we chose the α' set of quantum numbers of each atom's ground level to be in accordance to Hund's rules. These levels and the respective ionized levels are listed in Table 1. These ionized levels contain a change of total angular momentum from the respective ground state of 1/2 due to angular momentum conservation. Furthermore, the listed levels are the only ionization channels with relevant cross-sections.

We further investigated the contributions of the anisotropy and alignment parameters to the angular distribution. Although the nature of the distribution is fixed by the second-order Legendre polynomial, its amplitude is given by the multiplication of these two parameters. The values of the anisotropy coefficients α_2^{if} are listed in Table 2, for all the possible dipole transition combinations of J_i and J_f, from 0 to 9/2, in the four studied elements.

In the case of the alignment parameter $\mathcal{A}_2$, the calculation has to be performed for each α_i set of quantum numbers, with their respective cross sections. The values of these parameters for the K shell are listed in Table 1 for Cu, Co, Ni and Rh. We observe some variation between values of J_i within the same atomic system, while for same values of J_i deviations in the alignment are in the sixth digit, even for different atomic systems. Additionally, this parameter has a value of 0 for Cu

Table 3
Magnetic sublevel cross-sections (10^{-20} cm^2) calculated with FAC code and used in the calculation of the alignment parameters.

J_i	M_i	Cu	Co	Ni	Rh
0	0	0.020788	–	–	–
1	−1	0.041576	–	–	–
1	0	0.020788	–	–	–
1	1	0[a]	–	–	–
4	−4	–	0.026770	–	0.003329
4	−3	–	0.026770	–	0.003329
4	−2	–	0.026770	–	0.003329
4	−1	–	0.026770	–	0.003329
4	0	–	0.013385	–	0.001664
5	−5	–	0.026770	–	0.003329
5	−4	–	0.026770	–	0.003329
5	−3	–	0.026770	–	0.003329
5	−2	–	0.026770	–	0.003329
5	−1	–	0.026770	–	0.003329
5	0	–	0.013385	–	0.001664
7/2	−7/2	–	–	0.023673	–
7/2	−5/2	–	–	0.023674	–
7/2	−3/2	–	–	0.023673	–
7/2	−1/2	–	–	0.034196	–
9/2	−9/2	–	–	0.023674	–
9/2	−7/2	–	–	0.023673	–
9/2	−5/2	–	–	0.023674	–
9/2	−3/2	–	–	0.023673	–
9/2	−1/2	–	–	0.036826	–

[a]Within the table accuracy.

with $J_i = 0$, which is consistent with the anisotropy parameter's value when considering only dipole transitions. Moreover, we also observe an almost zero alignment for Cu with $J_i = 0$. Across the four atoms, we observe an increase of the absolute value of alignment parameter with the increase of J_i. The sign does not affect the amplitude of the angular distribution, only the orientation of the anisotropy. A positive sign corresponds to a perpendicular emission to the electron beam direction, while a negative sign is for the parallel case.

The values of the cross sections calculated with FAC that were used in the calculation of these parameters are listed in Table 3. Using these values, we can further understand the variations of the absolute value of the alignment parameter for each cases. The values that are not listed in the table are equal to the values for symmetric M_i's (up to the shown decimal place).

From Eq. (6) we can see that, although the summation is normalized to the total cross section, each magnetic sublevel cross section is multiplied by a value dependent on the level's J_i and sublevel's M_i. In Table 3 we note that although for Co and Ni the cross section values are similar, there are two major differences: The J_i value for Ni is half integer, resulting in one extra contribution to the summation, compared to Co where the value of J_i differs by only $1/2$. Secondly, in the case of Co the value of the cross section for $M_i = 0$ is lower than for the remaining sublevels, whereas in the case of Ni, the cross sections for $M_i = -1/2, 1/2$ are larger. Additionally, if the absolute value of M_i is close to 0, this will represent a larger contribution to the summation, compared to intermediate absolute values of M_i. For these intermediate values, the term $3M_i^2 - J_i(J_i+1)$ will be closer to 0, resulting in a smaller contribution.

The spectra without angular distribution, i.e. with isotropic emission are shown in Fig. 1. We obtained the Kα final spectra for the elements by multiplying each of the lines by their respective angular distributions, identified by the initial and final total angular momentum, J_i and J_f. For a closer look of the angular distribution, we plot in Fig. 2 the relative difference between 90° and 0°, as well as between isotropic and 0°. The case of Cu is not plotted because it is isotropic within the present accuracy.

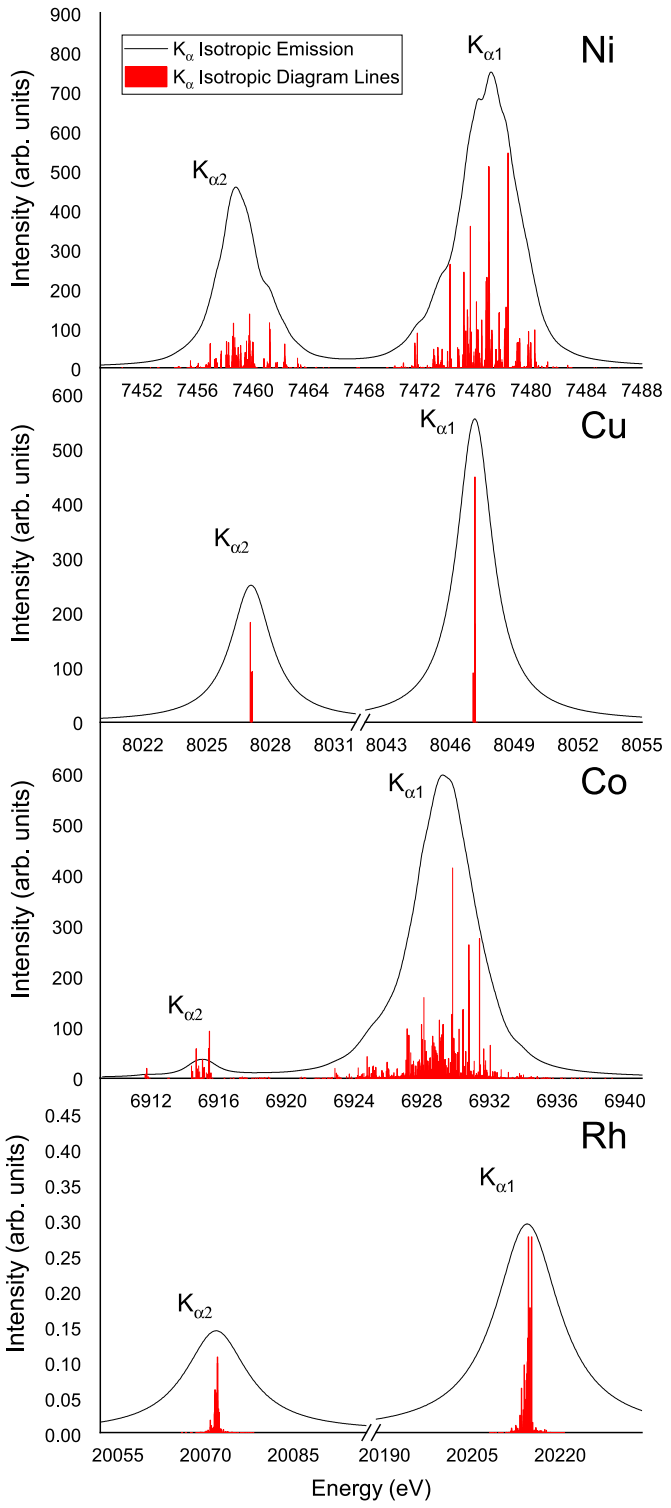

Fig. 1. Synthetic Isotropic spectra for Ni, Co and Rh for a K shell ionization. The respective diagram lines are represented in red.

The final calculated spectra show a total relative variation in intensity between 90° and 0° of approximately 1.3% for Ni, 1% for Co and 0.07% for Rh. Between isotropic emission and 0° this difference is 0.9% for Ni, 0.7% for Co and 0.05% for Rh. These differences are supported by the small values of the alignment parameters for each of the atoms and their respective ionization cross sections. Furthermore, each ionized state will decay for several final states with angular

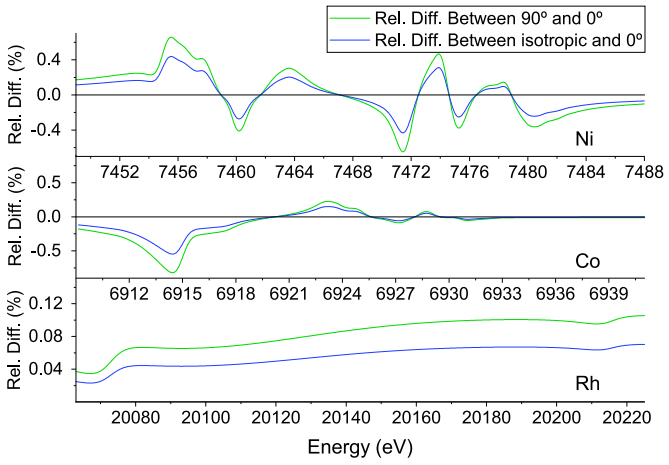

Fig. 2. Relative differences between the intensity at 90° and 0° (green) and between isotropic emission and 0° (blue).

momentum J_f, which according to Table 2 has different signs for α_2^{if}. This results in a cancellation of angular distributions of individual transitions with opposite directions, further suppressing the total angular distribution. This effect can be clearly observed by comparing the Co and Rh diagram line spectra where, although the value of the alignment parameters in these atoms are approximately equal, in Rh the anisotropy is reduced to less than 0.1%, due to the overlap of lines. Because of the higher atomic number of Rh, the respective lines are closely packed, while in Co they are more spread out. This leads to a smaller overlap for Co, and higher cancellation of respective different angular distribution.

4. Conclusion

We calculated the angular distribution of Kα emission in several atoms, namely Cu, Co, Rh and Ni, after electron impact ionization. For that purpose, the total emission was evaluated using atomic parameters of radiative and Auger rates, and level energies previously calculated with the MCDFGME code. For each Kα transition, we calculated the respective angular distribution with values of magnetic sub-level cross-sections evaluated with the FAC code. We concluded that the angular distributions for these elements is almost isotropic, being Ni the element with a maximum of angular asymmetry of about 0.7%. This is due to a small angular momentum of the ionized levels that leads to a small alignment parameters, as well as to a cancellation of the various angular distributions in the overlap of lines, which have opposite sign.

Declaration of competing interest

The authors declare that they have no known competing financial interests or personal relationships that could have appeared to influence the work reported in this paper.

Acknowledgements

This research was funded in part by FCT (Portugal) under research center grant UID/FIS/04559/2020 (LIBPhys). This work was also funded through the project PTDC/FIS-AQM/31969/2017, "Ultra-high-accuracy x-ray spectroscopy of transition metal oxides and rare earths." J. M and J.P.S acknowledge the support of EMPIR, Germany, under Contract No. 17FUN02MetroMMC. The EMPIR initiative is co-funded by the European Union's Horizon 2020 research and innovation programme and the EMPIR participating States.

References

Amaro, P., Shah, C., Steinbrügge, R., Beilmann, C., Bernitt, S., López-Urrutia, J.R., Tashenov, S., 2017. State-selective influence of the Breit interaction on the angular distribution of emitted photons following dielectronic recombination. Phys. Rev. A 95 (2), 1–10. http://dx.doi.org/10.1103/PhysRevA.95.022712.

Balashov, V.V., Grum-Grzhimailo, A.N., Kabachnik, N.M., 2000. Polarization and Correlation Phenomena in Atomic Collisions, first ed. Springer US, Boston, MA, pp. 107–131. http://dx.doi.org/10.1007/978-1-4757-3228-3.

Barrea, R.A., Pérez, C.A., Plivelic, T.S., Bonzi, E.V., Sánchez, H.J., 2005. Anisotropic angular distribution of Er L x-rays following photoionization by linearly polarized radiation. J. Phys. B: At. Mol. Opt. Phys. 38 (7), 839–852. http://dx.doi.org/10.1088/0953-4075/38/7/006.

Barros, S.F., Vanin, V.R., Mangiarotti, A., Maidana, N.L., Fernández-Varea, J.M., 2019. Atomic alignment of 73Ta, 74 W, and 79Au after L3 subshell ionization by 10-100-keV electron impact ATOMIC ALIGNMENT of TA 73, W 74, and ... SUELEN F. BARROS et al.. Phys. Rev. A 100 (6), 1–14. http://dx.doi.org/10.1103/PhysRevA.100.062705.

Blum, K., Kleinpoppen, H., 1979. Electron-photon angular correlation in atomic physics. Phys. Rep. 52 (4), 203–261. http://dx.doi.org/10.1016/0370-1573(79)90031-0.

Chen, Z.B., Dong, C.Z., 2018. Angular distribution and polarization of X-ray radiation in highly charged He-like ions: hyperfine-induced transition. Eur. Phys. J. D 72 (6), http://dx.doi.org/10.1140/epjd/e2018-90058-2.

Chen, M.H., Reed, K.J., 1994. Relativistic effects on angular distribution of Auger electrons emitted from Be-like ions following electron-impact excitation. Phys. Rev. A 50 (3), 2279–2283. http://dx.doi.org/10.1103/PhysRevA.50.2279.

Desclaux, J.P., 1975. A multiconfiguration relativistic DIRAC-FOCK program. Comput. Phys. Comm. 9 (1), 31–45. http://dx.doi.org/10.1016/0010-4655(75)90054-5.

Gonzales, D., Cavness, B., Williams, S., 2011. Angular distribution of thick-target bremsstrahlung produced by electrons with initial energies ranging from 10 to 20 keV incident on Ag. Phys. Rev. A - At., Mol., Opt. Phys. 84 (5), 1–5. http://dx.doi.org/10.1103/PhysRevA.84.052726.

Gu, M.F., 2008. The flexible atomic code. Can. J. Phys. 86 (5), 675–689. http://dx.doi.org/10.1139/P07-197.

Guerra, M., Amaro, P., Machado, J., Santos, J.P., 2015a. Single differential electron impact ionization cross sections in the binary-encounter-bethe approximation for the low binding energy regime. J. Phys. B: At. Mol. Opt. Phys. 48 (18), 185202. http://dx.doi.org/10.1088/0953-4075/48/18/185202.

Guerra, M., Parente, F., Indelicato, P., Santos, J.P., 2012. Modified binary encounter Bethe model for electron-impact ionization. Int. J. Mass Spectrom. 313, 1–7. http://dx.doi.org/10.1016/j.ijms.2011.12.003, arXiv:1306.2826.

Guerra, M., Sampaio, J.M., Madeira, T.I., Parente, F., Indelicato, P., Marques, J.P., Santos, J.P., Hoszowska, J., Dousse, J.C., Loperetti, L., Zeeshan, F., Müller, M., Unterumsberger, R., Beckhoff, B., 2015b. Theoretical and experimental determination of l -shell decay rates, line widths, and fluorescence yields in ge. Phys. Rev. A - At., Mol., Opt. Phys. 92 (2), 1–9. http://dx.doi.org/10.1103/PhysRevA.92.022507.

Guerra, M., Sampaio, J.M., Vília, G.R., Godinho, C.A., Pinheiro, D., Amaro, P., Marques, J.P., Machado, J., Indelicato, P., Parente, F., Santos, J.P., 2021. Fundamental parameters related to selenium Kα and Kβ emission X-ray spectra. Atoms 9 (1), 8. http://dx.doi.org/10.3390/atoms9010008.

Han, I., Demir, L., 2011. Angular dependence of L3-subshell X-ray emission following photoionisation. J. X-Ray Sci. Technol. 19 (1), 13–21. http://dx.doi.org/10.3233/XST-2010-0276.

Indelicato, P., Desclaux, J.P., 1990. Multiconfiguration Dirac-Fock calculations of transition energies with QED corrections in three-electron ions. Phys. Rev. A 42 (9), 5139–5149. http://dx.doi.org/10.1103/PhysRevA.42.5139, URL https://link.aps.org/doi/10.1103/PhysRevA.42.5139.

Indelicato, P., Santos, J.P., Boucard, S., Desclaux, J.-P., 2007. QED and relativistic corrections in superheavy elements. Eur. Phys. J. D 45 (1), 155–170. http://dx.doi.org/10.1140/epjd/e2007-00229-y, arXiv:0701160 URL http://link.springer.com/10.1140/epjd/e2007-00229-y.

Iorga, C., Stancalie, V., 2019. Linear polarization of the dielectronic recombination Kα satellite lines in Li-like Au76+. J. Quant. Spectrosc. Radiat. Transfer 224, 206–216. http://dx.doi.org/10.1016/j.jqsrt.2018.11.017.

Kabachnik, N.M., Sazhina, I.P., 1984. Angular distribution and spin polarisation of Auger electrons. J. Phys. B: At. Mol. Phys. 17 (7), 1335–1342. http://dx.doi.org/10.1088/0022-3700/17/7/017.

Karanfil, C., Barrea, R.A., 2011. Non-isotropic angular distribution of Yb Lα1 and Lα2 lines following photoionization by linearly polarized radiation. J. Phys. B: At. Mol. Opt. Phys. 44 (23), http://dx.doi.org/10.1088/0953-4075/44/23/235002.

Kumar, S., Sharma, V., Mehta, D., Singh, N., 2008. Alignment of Mi (i=3-5) subshell vacancy states in Au79, Bi83, Th90, and U92 following photoionization by unpolarized Mn K x rays. Phys. Rev. A - At., Mol., Opt. Phys. 77 (3), 1–11. http://dx.doi.org/10.1103/PhysRevA.77.032510.

Kust, H., Kleiman, U., Mehlhorn, W., 2003. Alignment after Xe L 3 photoionization by synchrotron radiation. J. Phys. B: At. Mol. Opt. Phys. 36 (10), 2073–2082. http://dx.doi.org/10.1088/0953-4075/36/10/315.

Liu, Y., Xu, Z., Wang, X., Zeng, L., 2019. Angular dependence of Ag L-X-rays emission induced by 20–40 keV electron-impact. Nucl. Instrum. Methods Phys. Res., B 446 (March), 1–4. http://dx.doi.org/10.1016/j.nimb.2019.03.019.

Löwdin, P.O., 1955. Quantum theory of many-particle systems. I. Physical interpretations by means of density matrices, natural spin-orbitals, and convergence problems in the method of configurational interaction. Phys. Rev. 97 (6), 1474–1489. http://dx.doi.org/10.1103/PhysRev.97.1474.

Martins, L., Amaro, P., Pessanha, S., Guerra, M., Machado, J., Carvalho, M.L., Santos, J.P., 2020a. Multiconfiguration Dirac–Fock calculations of Zn K-shell radiative and nonradiative transitions. X-Ray Spectrom. 49 (1), 192–199. http://dx.doi.org/10.1002/xrs.3089.

Martins, L., Amaro, P., Pessanha, S., Guerra, M., Machado, J., Carvalho, M.L., Santos, J.P., 2020b. Multiconfiguration Dirac–Fock calculations of Zn K-shell radiative and nonradiative transitions. X-Ray Spectrom. 49 (1), 192–199. http://dx.doi.org/10.1002/xrs.3089.

Ménesguen, Y., Lépy, M.-C., Hönicke, P., Müller, M., Unterumsberger, R., Beckhoff, B., Hoszowska, J., Dousse, J.-C., Błachucki, W., Ito, Y., Yamashita, M., Fukushima, S., 2018. Experimental determination of the x-ray atomic fundamental parameters of nickel. Metrologia 55 (1), 56–66. http://dx.doi.org/10.1088/1681-7575/aa9b12.

Nakamura, N., Hu, Z., Watanabe, H., Li, Y., Kato, D., Currell, F.J., Tong, X.M., Watanabe, T., Ohtani, S., 2011. Structure and dynamics of highly charged heavy ions studied with the electron beam ion trap in Tokyo. Hyperfine Interact. 199 (1), 123–130. http://dx.doi.org/10.1007/s10751-011-0307-7.

Namito, Y., Ban, S., Hirayama, H., 2008. Azimuthal-angle dependence of L x-ray intensity following photoionization of Pb, Au, and W atoms by a linearly polarized photon. Phys. Rev. A - At., Mol., Opt. Phys. 78 (3), 1–8. http://dx.doi.org/10.1103/PhysRevA.78.033419.

Nishimura, H., Danjo, A., Takahashi, A., 1986. Electron-photon angular correlations for electron impact excitation of Xe. J. Phys. B: At. Mol. Phys. 19 (5), http://dx.doi.org/10.1088/0022-3700/19/5/009.

Rousseau, R.M., 2001. Detection limit and estimate of uncertainty of analytical XRF results. Rigaku J. 18 (2), 33–47.

Sampaio, J.M., Madeira, T.I., Marques, J.P., Parente, F., Costa, A.M., Indelicato, P., Santos, J.P., Lépy, M.C., Ménesguen, Y., 2014. Approaches for theoretical and experimental determinations of K -shell decay rates and fluorescence yields in Ge. Phys. Rev. A - At., Mol., Opt. Phys. 89 (1), 1–8. http://dx.doi.org/10.1103/PhysRevA.89.012512.

Santos, J.P., Parente, F., Boucard, S., Indelicato, P., Desclaux, J.P., 2005. X-ray energies of circular transitions and electron screening in kaonic atoms. Phys. Rev. A 71 (3), 032501. http://dx.doi.org/10.1103/PhysRevA.71.032501, URL https://link.aps.org/doi/10.1103/PhysRevA.71.032501.

Santra, S., Mitra, D., Sarkar, M., Bhattacharya, D., 2007. Angular distribution of Au and U L x rays induced by 22.6-keV photons. Phys. Rev. A - At., Mol., Opt. Phys. 75 (2), 1–7. http://dx.doi.org/10.1103/PhysRevA.75.022901.

Schmidt, V., 1992. Photoionization of atoms using synchrotron radiation. Rep. Progr. Phys. 55 (9), 1483–1659. http://dx.doi.org/10.1088/0034-4885/55/9/003.

Scofield, J.H., 1976. Angular dependence of fluorescent x rays. Phys. Rev. A 14 (4), 1418–1420. http://dx.doi.org/10.1103/PhysRevA.14.1418.

Sestric, G., Ferguson, S., Wright, I., Williams, S., 2014. Angular distributions of X-rays emitted following L3 ionization of Au atoms by electron impact. Radiat. Phys. Chem. 102, 40–43. http://dx.doi.org/10.1016/j.radphyschem.2014.04.024.

Shah, C., Amaro, P., Steinbrügge, R., Bernitt, S., López-Urrutia, J.R.C., Tashenov, S., 2018. Polarization of K-shell dielectronic recombination satellite lines of Fe xix–xxv and its application for diagnostics of anisotropies of hot plasmas. Astrophys. J. Suppl. Ser. 234 (2), 27. http://dx.doi.org/10.3847/1538-4365/aaa4c0, arXiv:1801.01888.

Sharma, L., Surzhykov, A., Inal, M.K., Fritzsche, S., 2010. Polarization transfer in the inner-shell photoionization of sodiumlike ions. Phys. Rev. A - At., Mol., Opt. Phys. 81 (2), 1–11. http://dx.doi.org/10.1103/PhysRevA.81.023419.

Singh, B., Kumar, S., Prajapati, S., Singh, B.K., Llovet, X., Shanker, R., 2017. Measurement of angular distributions of K x-ray intensity of Ti and Cu thick targets following impact of 10–25 keV electrons. J. Electron Spectrosc. Relat. Phenom. 216, 17–22. http://dx.doi.org/10.1016/j.elspec.2017.02.002.

Tartari, A., Baraldi, C., Casnati, E., Re, A.D., Fernandez, J.E., Taioli, S., 2003. On the angular dependence of L x-ray production cross sections following photoionization at an energy of 59.54 keV. J. Phys. B: At. Mol. Opt. Phys. 36 (5), 843–851. http://dx.doi.org/10.1088/0953-4075/36/5/305.

Tashenov, S., Stöhlker, T., Banas, D., Beckert, K., Beller, P., Beyer, H.F., Bosch, F., Fritzsche, S., Gumberidze, A., Hagmann, S., Kozhuharov, C., Krings, T., Liesen, D., Nolden, F., Protic, D., Sierpowski, D., Spillmann, U., Steck, M., Surzhykov, A., 2006. First measurement of the linear polarization of radiative electron capture transitions. Phys. Rev. Lett. 97 (22), 1–4. http://dx.doi.org/10.1103/PhysRevLett.97.223202.

Tulkki, J., Kabachnik, N.M., Aksela, H., 1993. Effects of channel interaction, exchange, and relaxation on the angular distribution and spin polarization of Auger electrons from noble-gas atoms. Phys. Rev. A 48 (2), 1277–1291. http://dx.doi.org/10.1103/PhysRevA.48.1277.

Wang, X., Xu, Z., Zhang, Y., Ma, C., Zhu, C., 2016. Angular dependence of L X-rays emission for Ag by 10 keV electron-impact. Radiat. Phys. Chem. 125, 102–105. http://dx.doi.org/10.1016/j.radphyschem.2016.03.023.

Wu, Z.W., Surzhykov, A., Fritzsche, S., 2014. Hyperfine-induced modifications to the angular distribution of the K α 1 x-ray emission. Phys. Rev. A - At., Mol., Opt. Phys. 89 (2), 1–7. http://dx.doi.org/10.1103/PhysRevA.89.022513.

Wu, Z.W., Tian, Z.Q., An, Y.H., Dong, C.Z., 2021. Angular distribution and polarization of the 3C and 3D lines following electron-impact excitation of Fe 16+ Ions. Astrophys. J. 910 (2), 142. http://dx.doi.org/10.3847/1538-4357/abe7f2.

Wu, Z.W., Tian, Z.Q., Jiang, J., Dong, C.Z., Fritzsche, S., 2020. Hyperfine-induced effects on angular emission of the magnetic-quadrupole line 1s2p3/2 P2 3 → 1s2 S0 1 following electron-impact excitation of Tl79+ ions. Phys. Rev. A 102 (4), 1–8. http://dx.doi.org/10.1103/PhysRevA.102.042813.

Yamaoka, H., Oura, M., Takahiro, K., Takeshima, N., Kawatsura, K., Mizumaki, M., Kleiman, U., Kabachnik, N.M., Mukoyama, T., 2002. Angular distribution of Au and Pb L x rays following photoionization by synchrotron radiation. Phys. Rev. A - At., Mol., Opt. Phys. 65 (6), 627131–627138. http://dx.doi.org/10.1103/PhysRevA.65.062713.

Zhang, D.H., Dong, C.Z., Wu, Z.W., 2020. Angular distribution and polarization of characteristic x-ray lines following innershell photoionization of tungsten by linearly polarized light. J. Quant. Spectrosc. Radiat. Transfer 244, http://dx.doi.org/10.1016/j.jqsrt.2020.106844.